AGU PUBLICATIONS

Journal of Advances in Modeling Earth Systems

RESEARCH ARTICLE

10.1002/2013MS000284

Key Points:
- The SPITFIRE fire model was evaluated within the JSBACH land surface model
- A modified wind speed response improved the spatial pattern of burned area
- Regional gradients in burned area are driven by vegetation and fuel properties

Correspondence to:
G. Lasslop,
gitta.lasslop@mpimet.mpg.de

Citation:
Lasslop, G., K. Thonicke, and S. Kloster (2014), SPITFIRE within the MPI Earth system model: Model development and evaluation, *J. Adv. Model. Earth Syst.*, *6*, 740–755, doi:10.1002/2013MS000284.

Received 20 NOV 2013
Accepted 2 JUL 2014
Accepted article online 8 JUL 2014
Published online 5 AUG 2014
Corrected 29 SEP 2014

This article was corrected on 29 SEP 2014. See the end of the full text for details.

SPITFIRE within the MPI Earth system model: Model development and evaluation

Gitta Lasslop[1], Kirsten Thonicke[2], and Silvia Kloster[1]

[1]Max Planck Institute for Meteorology, Fire in the Earth System, Land in the Earth System, Hamburg, Germany, [2]Potsdam Institute for Climate Impact Research (PIK) e.V., Earth System Analysis, Research Domain 1, Ecosystem Stability and Transitions, Potsdam, Germany

Abstract Quantification of the role of fire within the Earth system requires an adequate representation of fire as a climate-controlled process within an Earth system model. To be able to address questions on the interaction between fire and the Earth system, we implemented the mechanistic fire model SPITFIRE, in JSBACH, the land surface model of the MPI Earth system model. Here, we document the model implementation as well as model modifications. We evaluate our model results by comparing the simulation to the GFED version 3 satellite-based data set. In addition, we assess the sensitivity of the model to the meteorological forcing and to the spatial variability of a number of fire relevant model parameters. A first comparison of model results with burned area observations showed a strong correlation of the residuals with wind speed. Further analysis revealed that the response of the fire spread to wind speed was too strong for the application on global scale. Therefore, we developed an improved parametrization to account for this effect. The evaluation of the improved model shows that the model is able to capture the global gradients and the seasonality of burned area. Some areas of model-data mismatch can be explained by differences in vegetation cover compared to observations. We achieve benchmarking scores comparable to other state-of-the-art fire models. The global total burned area is sensitive to the meteorological forcing. Adjustment of parameters leads to similar model results for both forcing data sets with respect to spatial and seasonal patterns.

1. Introduction

Fire is an integral part of the Earth system affecting various components through a variety of fire-mediated processes [*Bowman et al*., 2009; *Keywood et al*., 2013]. Modeling fire occurrence and spread on the global scale is a challenging task due to the influence of many factors, which are themselves often difficult to quantify (e.g., human ignitions, fuel load, fuel moisture). Due to interactions between the influencing factors, a change in one factor can lead to a positive response of burned area in one region and a negative response in a second region. For instance, a decrease in precipitation can lead to increases of burned area due to higher flammability or to a reduction due to the indirect effect of precipitation on biomass which can cause a lack of fuel [*Krawchuk and Moritz*, 2011]. Moreover, fire changes a number of land surface properties, e.g., the albedo or the vegetation type and structure which determine the energy and carbon fluxes between land and atmosphere and consequently impact the climate system [*Bowman et al*., 2009].

Quantification of the impacts of fire on the Earth system therefore requires a mechanistic representation of the processes related to fire within an Earth system model. We implemented SPITFIRE [*Thonicke et al*., 2010], a mechanistic global fire model, in JSBACH, the land surface component of the MPI Earth system model (MPI-ESM). The SPITFIRE model is the most complex fire model applied in global models so far. This model is well suited for application in an Earth system model which is applied under a wide range of climatic conditions. For instance, the fireline intensity is a prognostic variable, while it is not modeled in other approaches. This variable will be useful for improving the representation of the fire effects on the atmosphere. The simulated vegetation distribution is strongly influenced by fire. In SPITFIRE, the tree mortality varies according to fire and vegetation characteristics, in more simple approaches mortality is a constant parameter per plant functional type [*Arora and Boer*, 2005]. SPITFIRE has been included in other vegetation models [*Lehsten et al*., 2009; *Prentice et al*., 2011; *Pfeiffer et al*., 2013], but so far not within an Earth system model. The implementation within an Earth system model will in future allow us to analyze the influences of fire on the climate system as well as feedbacks between climate and fire. The influence of fire on the

Earth system is not part of this study. The objective of the present study is to document the model and to perform an evaluation including sensitivity tests. Within the MPI-ESM, the model will be applied under different climatic settings. A good understanding of the sensitivities and shortcomings of the model will be the basis for interpreting the results of such simulations.

SPITFIRE is driven by meteorological conditions, vegetation cover, fuel load, and fuel properties. The fire algorithm is therefore expected to be sensitive to the meteorological forcing. To analyze this uncertainty, we force the model with two observationally based meteorological forcing data sets and evaluate the outcome with respect to spatial patterns and seasonality of burned area and carbon emissions. SPITFIRE includes the basic processes of fire occurrence and fire spread. So far the influence of wind speed on fire has been considered in models by increasing the rate of spread with increasing wind speed [*Thonicke et al*., 2010; *Prentice et al*., 2011; *Pfeiffer et al*., 2013]. In some approaches, the influence of wind speed is not increased further when a certain limit of wind speed is reached [*Rothermel*, 1972; *Arora and Boer*, 2005; *Kloster et al*., 2010; *Li et al*., 2012, 2014]. Wind speed influences the flame angle and can improve the transfer of heat to the surrounding fuel. When a certain wind speed threshold is reached, higher wind speed is no longer beneficial for fire spread. We adjust the influence of wind speed in our model to improve the relation between wind speed and burned fraction in comparison to observational data. We evaluate the model using remote sensing data and analyze the residuals with respect to driving variables of the model. SPITFIRE is currently applied in a number of global vegetation models [*Thonicke et al*., 2010; *Prentice et al*., 2011; *Pfeiffer et al*., 2013; *Yue et al*., 2014]. We build our work on the original SPITFIRE LPJ implementation [*Thonicke et al*., 2010]. Parameters of the SPITFIRE model are changed to decrease the difference between simulated and observed burned area. We do not compare the JSBACH-SPITFIRE implementations to other SPITFIRE implementation, as the current study does not aim for a model intercomparison, but for a documentation of the implementation of SPITFIRE into the MPI-ESM. In the last part of the paper, we analyze the influence of selected variables on the spatial variation of the modeled burned area.

2. Methods

In this section, we describe the implementation of SPITFIRE within the land surface model JSBACH, as well as the modifications with respect to wind speed. The data sets used for model forcing and evaluation are described in the following section and the final section covers the set up of the model simulations.

2.1. Model and Modifications

We used the JSBACH land surface model [*Brovkin et al*., 2013; *Raddatz et al*., 2007; *Reick et al*., 2013; *Schneck et al*., 2013] which is the land component of the MPI-ESM [*Giorgetta et al*., 2013]. The model includes process-based representations of the carbon and hydrological cycle. Our model version was updated since the model version of the CMIP5 (Coupled Model Intercomparison Project Phase 5) experiments [*Reick et al*., 2013] to include a five layer soil hydrology scheme [*Hagemann and Stacke,* 2014]. In this version of the model, we included the mechanistic fire model SPITFIRE [*Thonicke et al*., 2010]. The following variables are used as input for the SPITFIRE algorithm: precipitation, daily temperature minimum and maximum, wind speed, soil moisture of the surface soil layer, carbon content of the vegetation and litter pools, and the vegetation distribution. According to the burned fraction and postfire mortality of trees, SPITFIRE computes carbon emissions due to fire and redistributes the carbon pools. Vegetation distribution in 1850 was prescribed by cover fractions for each plant functional type (PFT) and a desert fraction. The vegetation distribution is then updated every year according to the land use transitions provided by *Hurtt et al*. [2011]. The implementation of the anthropogenic land use scheme is described in detail in *Reick et al*. [2013]. From a historical run (1850–2005) with JSBACH, we extracted the forcing data to drive a reduced carbon pool model version [CBALONE, *Schneck et al*., 2013], which consists of the carbon allocation scheme of JSBACH including anthropogenic land use and disturbances. This model version was forced with PFT-specific net primary productivity (NPP) and LAI, as well as soil temperature and relative soil moisture plus the variables required by SPITFIRE. NPP prescribed here is shown in Figure 1. CBALONE is able to reproduce identical results to simulations with the full JSBACH model. Thus, experiments related to the land carbon cycle can be performed by running CBALONE only, which requires much less computational resources than the same experiments using the entire JSBACH or even the MPI-ESM.

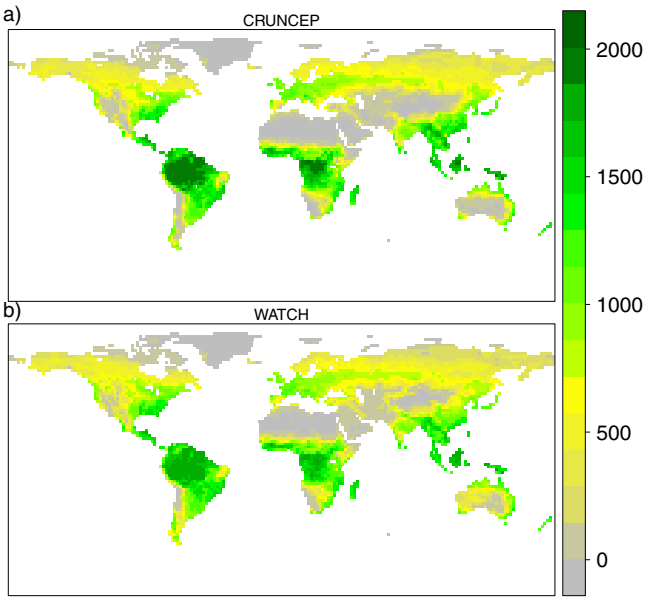

Figure 1. JSBACH annual NPP (g C m^{-2}) forced with CRUNCEP (a) and WATCH (b) meteorological data set.

2.1.1. Modifications of SPITFIRE

SPITFIRE as documented in *Thonicke et al.* [2010] was developed for the use within the LPJ vegetation model. We subsequently implemented it in JSBACH. Some adjustments were necessary to adapt the algorithm to the JSBACH land surface model. JSBACH uses two shrub PFTs while LPJ does not include shrub PFTs. The parameters for the two additional PFTs were assumed to be comparable to the temperate broadleaved summer green type of *Thonicke et al.* [2010] for the deciduous shrubs and to the tropical broadleaved rain green tree for the rain green shrubs. The fuel bulk density of shrubs was set to the average value of *Marino et al.* [2012] (5 kg m^{-2}) and the crown length was set to 0.8. The other PFTs were comparable to the PFTs used in LPJ. The PFT-specific parameters are listed in Table 1.

JSBACH did not include a computation of vegetation height, which is necessary for SPITFIRE for the computation of tree mortality. To estimate the vegetation height, we followed *Shevliakova et al.* [2009]:

$$height_{veg} = hmax * (1.0 - exp(-hl * BM) \quad (1)$$

$height_{veg}$ (m) is the vegetation height, *hmax* ($2.419 \cdot 10^1$ m) and *hl* (0.19 $m^2(kgC)^{-1}$) are constant parameters and BM is the living biomass (kg m^{-2}) (consisting of wood, green and reserve carbon pools in JSBACH). The equation is used for all woody PFTs. JSBACH performs the computations for fire spread and occurrence for the part of the grid cell covered with vegetation that is allowed to burn, i.e., carbon pools are used per m^2 of vegetated area not per m^2 of the grid cell. Subsequently it scales the fire fraction to the whole grid cell, accounting for the actual fraction that can burn. This excludes nonvegetated areas and croplands, with croplands updated every year according to *Hurtt et al.* [2011].

The burned fraction is computed as the product of the burned fraction per fire multiplied by the number of fires. Fires can be ignited by either lightning or humans. Ignitions due to lightning are determined based on

Table 1. Parameters Used in the Model Specified for the Plant Functional Types Used in the Model Runs[a]

PFT	me (-)	FBD (kg m^{-3})	Scorch Height Parameter (-)	Crown Length Parameter (-)	par1 (-)	par2 (-)	Rck (-)	p (-)
Tropical evergreen trees	0.2	25	0.1478	0.33	0.0301	0.0281	1.0	3
Tropical deciduous trees	0.3	25	0.061	0.1	0.1085	0.0281	0.05	3
Extra-tropical evergreen trees	0.3	20	0.1	0.33	0.0367	0.0592	1	3.75
Extra-tropical deciduous trees	0.3	22	0.371	0.33	0.0347	0.1086	1	3
Raingreen shrubs	0.3	5	0.094	0.8	0.1085	0.212	1	3
Deciduous shrubs	0.3	5	0.094	0.8	0.0347	0.1086	1	3
C3 grass	0.2	2	-	-	-	-	-	-
C4 grass	0.2	2	-	-	-	-	-	-
C3 pasture	0.2	4	-	-	-	-	-	-
C4 pasture	0.2	4	-	-	-	-	-	-

[a]PFT: plant functional type, me: moisture of extinction, FBD: fuel bulk density, flame length: parameter used in the computation of the flame length, crown length: crown length divided by tree height, par1 and par2: bark thickness parameters, Rck and p: crown damage parameters. For descriptions of the parameters, see *Thonicke et al.* [2010].

flash rates, while human-caused ignitions are based on population density and a regionally varying factor ($a(N_D)$ A. Spessa, personal communication, 2013). We use the population density data set by *Klein Goldewijk* [2001]. Flash rates are based on the Lightning Imaging Sensor/Optical Transient Detector (LIS/OTD). The LIS/OTD product of the NASA LIS/OTD Science Team is available from the Global Hydrology Resource Center (http://ghrc.msfc.nasa.gov). This product reports total flashes. We used a latitude-dependent relation between total flashes and cloud-to-ground flashes to derive the cloud to ground fraction [*Pierce*, 1970]. This differs from *Thonicke et al*. [2010] who use a constant fraction. The sum of the human and lightning ignitions is reduced according to the fire danger index (FDI) to scale the potential fires to actual fires.

The burned fraction is computed based on the rate of spread according to *Rothermel* [1972] and assuming an elliptical shape of the area burned. The Rothermel equations use four classes of fuels differentiated according to their size. Fire intensity needs to reach a threshold to allow the fire to spread. Fire intensity and vegetation type determine the postfire mortality of trees. Mortality can occur due to tree crown or cambial damage. The combustion completeness and carbon emissions are computed depending on moisture and fuel properties.

The exact equations of the model can be found in *Thonicke et al*. [2010], we only specify our modifications in detail here. For the human ignitions ($n_{h,ig}$), we use the equation of *Thonicke et al*. [2010].

$$n_{h,ig} = pop_{dens} k e^{-0.5\sqrt{pop_{dens}}} a(N_D), \tag{2}$$

but modify the parameter k to 0.65 to adjust the global burned area to the satellite-based observations. The value of k in *Thonicke et al*. [2010] was 30. This difference is most likely due to differences between the amounts of fuel and moisture in LPJ and JSBACH. The five -layer hydrology scheme has been evaluated recently (Hagemann and Stacke, submitted manuscript). The two models differ with respect to the number of layers in the hydrology scheme (five layers in JSBACH compared to two layers in LPJ) and with respect to the definitions of their carbon pools [*Raddatz et al*., 2007; *Sitch et al*., 2003]. We will not resolve the differences between the two models further here. The unit of the population density (pop_{dens}) is individuals per km^2, $a(N_D)$ is the propensity of humans to ignite a fire, its value varies regionally between $1.1 \cdot 10^{-3}$ and $3.29 \cdot 10^{-3}$ individual^{-1} day^{-1}. The function is zero at zero population density, has a maximum at 16 individuals per km^2 and approaches zero for high population densities.

To conserve the total burned area without changing the contribution of lightning and human ignitions to the total number of ignitions, we included a parameter to adjust the total number of ignitions directly. The total number of ignitions is the sum of human and lightning-caused ignitions.

In addition, we adjusted a parameter related to the fuel moisture. The fuel drying parameters lead to large areas with zero fire danger index. Consequently simulated burned area in boreal regions was too low. Increasing these parameters improved the fire patterns in the high latitudes. Proportionality of the drying parameters to the surface area to volume ratio was conserved. The ratio was $6.6 \cdot 10^4$ in the original code and was adjusted to $1.3 \cdot 10^4$.

We included a decrease of the wind speed multiplier, used to calculate the rate of spread, for high wind speeds. In the standard model, we found too high burned fractions compared to the observations in regions with high wind speed as a result of very high simulated rate of spread. Changes in modeled burned fraction due to this modification are shown in the results section (see section 3.1). The forward rate of spread (ROS_f) is computed based on the Rothermel equations:

$$ROS_f = \frac{I_R \xi (1 + \Phi_w)}{\rho_b \varepsilon Q_{ig}}, \tag{3}$$

where I_R (kJ m^{-2} min^{-1}) is the reaction intensity at the fire front, ξ, the propagating flux ratio, is the proportion of I_R that heats the adjacent fuel particles to ignition. Φ_w accounts for the effect of wind (wind speed multiplier). ρ_b (kg m^{-3}) is the bulk density of the fuel, ε is the proportion of a fuel particle that needs to be heated to ignition temperature to start flaming combustion, and Q_{ig} (kJ kg^{-1}) is the amount of heat required to ignite a given mass of fuel. The numerator is the amount of energy available to heat fuel while

the denominator is the energy required to heat the fuel to the point of ignition. We modified Φ_w by including an optimum wind speed, for higher wind speeds the value of Φ_w decreases linearly to zero. The further derivation of the burned fraction follows exactly the description in *Thonicke et al.* [2010] and references therein.

2.2. Data and Benchmarking Metrics

We used two meteorological forcing data sets to drive the model:

1. CRUNCEP as available from http://dods.extra.cea.fr/data/p529viov/cruncep/ (v4, 2011) for the years 1900–2005 and

2. the WATCH forcing data set for the years 1979–2005 [*Weedon et al.*, 2011].

The data sets include air temperature and humidity, shortwave and long-wave incident radiation, precipitation, and surface wind speed. These data sets were aggregated to a daily time step and T63 spatial resolution (1.875° × 1.875°). Annual atmospheric CO_2 was derived from a merged product of ice core [*Etheridge et al.*, 1996] and NOAA monitoring station data [*Keeling et al.*, 2005] for the years 1850–2005 [*Sitch et al.*, 2013]. The model evaluation is based on the GFED3 data sets of burned area [*Giglio et al.*, 2010] and carbon emissions [*van der Werf et al.*, 2010]. The GFED data are available online (http://www.globalfiredata.org/Data/index.html) in monthly and 0.5°× 0.5° resolution and were used here for the years 1997–2005. The spatial resolution was remapped to the resolution of the model (1.875°× 1.875°). The carbon emissions of the GFED3 database are separated into different sources. For our model-data comparison, we excluded the emissions due to deforestation, agricultural, or peatland fires as they are not included in the model. The burned area data set also specifies the burned area of different land cover types, but peatland and deforestation fires are not specified, and only croplands could be excluded for this data set. Peatland and deforestation fires have high carbon emissions for relatively small areas burned, therefore it is more important to exclude them when comparing the emissions.

We use the global benchmarking metrics for burned fraction as suggested by *Kelley et al.* [2013]. For completeness, we report the equations used here. They use the normalized mean error (NME, equation (4)) and normalized mean squared error (NMSE, equation (5)) to evaluate the spatial distribution.

$$NME = \frac{\sum_i |mod_i - obs_i|}{\sum_i |obs_i - \overline{obs}|}, \tag{4}$$

$$NMSE = \frac{\sum_i (mod_i - obs_i)^2}{\sum_i (obs_i - \overline{obs})^2}, \tag{5}$$

with *mod* being the modeled value and *obs* the observed and *i* the number of grid boxes. If the metrics are zero model and observations agree perfectly, if the metric is larger than one the model performs worse than the observational mean. In addition, the seasonality in terms of seasonal concentration and phase is included in the benchmarking metric. *Kelley et al.* [2013] quantify the seasonality by representing each data point as a vector, where the month is transformed into an angle

$$\theta_t = 2\pi(month - 1)/12 \tag{6}$$

and the length of the vector is given by the value of the data point, x_t, *t* indicates the time, i.e., the month. Then the sum of the vector components, *Lx* and *Ly* (equation (7)), can be computed as:

$$Lx = \sum_t x_t cos(\theta_t) \; and \; Ly = \sum_t x_t sin(\theta_t). \tag{7}$$

Based on this vector, the ratio of the length of the vector sum and the annual sum of the data points is interpreted as seasonal concentration

Table 2. List of Simulations With Parameters Used in the Model[a]

Model Run	ign	$wind_{max}$ (ft min^{-1})	Wind Decrease	Constant	Value
CRUNCEP no windlim	0.05	-	-	-	-
WATCHno no windlim	0.014	-	-	-	-
CRUNCEP windlim	1.0	100	0.5	-	-
WATCH windlim	0.55	150	0.5	-	-
WATCH wind CRUNCEP	0.74	100	0.5	-	-
Nfire constant	1.0	100	0.5	Number of fires	0.00002 ign ha^{-1}
Fuel constant	1.0	100	0.5	1—1000 h fuel	78 g biomass m^{-2}
FDI constant	1.0	100	0.5	FDI	0.91
Grass constant	0.175	100	0.5	Grass cover	1

[a]WATCH and CRUNCEP are the two forcing data sets, nfire is the number of fires, FDI the fire danger index.

$$C = \frac{\sqrt{Lx^2 + Ly^2}}{\sum_t x_t}. \tag{8}$$

while the direction of the vector represents the phase (P)

$$P = arctan(Lx/Ly). \tag{9}$$

The difference in seasonal concentration is quantified by NME and NMSE, while the difference in phase is quantified using the mean phase difference (MPD):

$$MPD = (1/\pi) arccos(cos(P_{mod} - P_{obs})/n). \tag{10}$$

2.3. Model Simulations

We performed spin-up simulations to equilibrate the carbon pools (except for the slow carbon pool which does not interact with the fire variables analyzed here), followed by transient model runs starting in 1850 until 2005. The CO_2 concentration includes the global increase starting from 1850. The years from 1850 until the start of the forcing data sets were filled with random years from 1901 to 1920 for the CRUNCEP data set. For the WATCH data set, the years from 1980 to 1999 were used repeatedly. For all simulations, the land use change transitions and harvest rates were prescribed according to *Hurtt et al.* [2011]. We performed runs with and without the wind limitation using both forcing data sets. We tuned the most uncertain process in the model, the human ignitions, for the simulation with wind speed limitation forced with the CRUNCEP data set, to match the global burned area of GFED for the years 1997–2005 (without burned croplands). For the simulation forced with WATCH data, with and without wind limitation, as well as the simulation forced with CRUNCEP without wind limitation, both ignition sources were tuned such that the contribution of lightning compared to human ignitions remained the same between the simulations. The differences in the spatial pattern are then not influenced by higher or lower proportions of one ignition source. All simulations and the parameter values used are listed in Table 2).

We estimate the influence of the wind speed on the difference between the simulations forced with CRUNCEP and WATCH. For this, we performed one simulation exchanging the wind speed and wind limitation parameters of the WATCH forcing with wind speed and limitation parameters of the CRUNCEP data set with the model version including the wind limitation.

In addition, we performed simulations with certain model parameters fixed to a globally constant value to investigate the sensitivity of the spatial patterns to these parameters. These model parameters were: the number of potential fires, vegetation distribution (we used only grass PFTs, but include the distribution of C3 and C4 grasses, pastures, and croplands in that case), the amount and composition of fuels, and the fire danger index. The value of these constant variables (except for the grass only run) were set to a value that yields a similar global burned area with all model parameters remaining the same (Table 2). For the model simulation using grass PFTs, only the ignitions were adjusted. These four simulations were performed using the wind limitation and the CRUNCEP forcing.

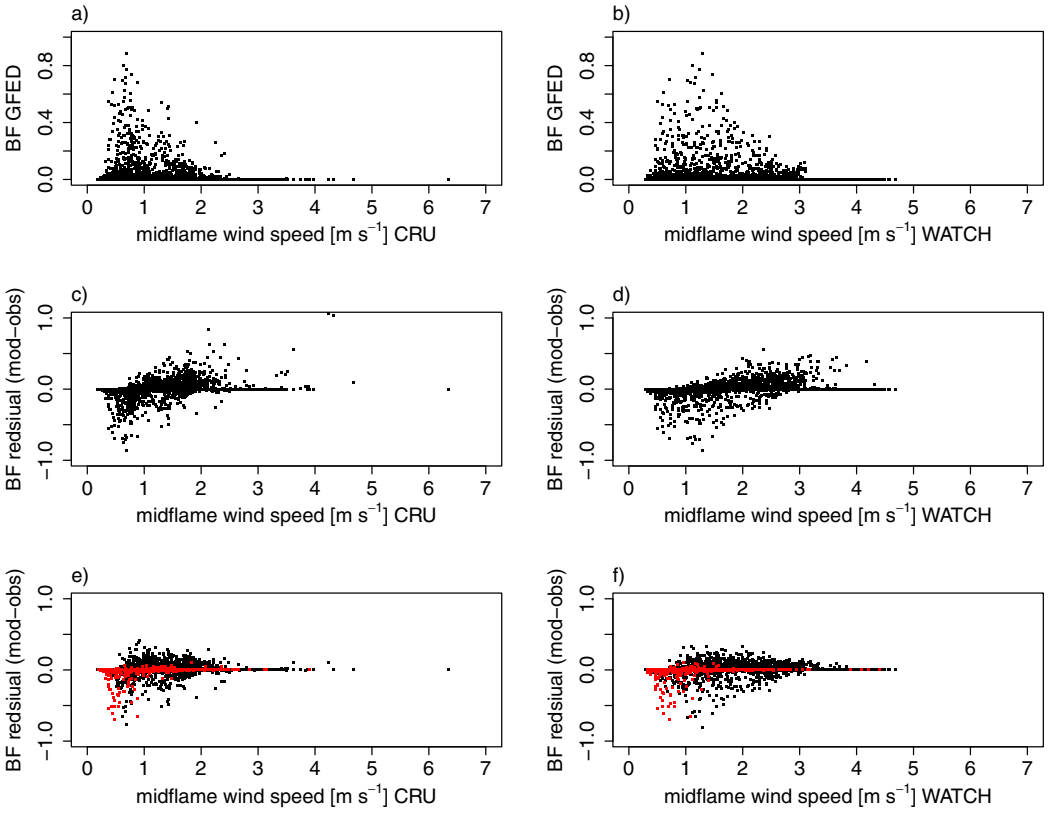

Figure 2. Annual burned fraction (BF) versus midflame wind speed (a, b), residual of annual burned fraction versus midflame wind speed without (c, d) and with (e, f) limitation. Left column (a, c, and e) are using the CRUNCEP forcing data, right column (b, d, f) are using WATCH forcing data. Red points indicate overestimation (>0.2) of the tree cover fraction in the model compared to *Hansen et al*. [2003].

3. Results and Discussion

3.1. Model Improvements With Respect to Wind Speed

This section focuses on the relation between wind speed and burned fraction. Wind speed has not been considered so far in studies analyzing observations about the spatial distribution of burned fraction. For the GFED3 data set of burned fraction, we find that high fractions of burned area occur only in a certain range of wind speed, expressed as midflame wind speed (see Figures 2a and 2b). This range differs between CRUNCEP and WATCH, fires occur with higher wind speed using the WATCH data set (CRUNCEP: up to 2.5 m s^{-1}, WATCH: up to 3 m s^{-1} for annual mean wind speed). For both data sets, the burned fraction shows a peak and a decrease for higher wind speed (see Figures 2a and 2b). The fire spread equations of *Thonicke et al*. [2010] include the positive effect of wind speed on fire spread but not the maximum rate of spread for high wind speed values suggested by *Rothermel* [1972]. Without a limitation on the wind speed multiplier, the model residuals (differences between model and observations) show a correlation with wind speed for both forcing data sets (see Figures 2c and 2d). Supported by the relation of GFED3 burned area with wind speed, we included a linear function that reduces the wind speed multiplier (see equation (3)) and therefore the rate of spread for wind speeds higher than a certain threshold. The threshold and strength of the decrease need to be adjusted to the wind speed forcing data (see Table 2). As a result, the overestimation of the burned fraction with high wind speed is strongly reduced when including this modification (see Figures 2e and 2f).

The number of potential fires, the sum of human- and lightning-caused ignitions, were tuned to yield a similar global burned area to be able to compare the spatial distribution for all experiments (Table 2). When including the wind limitation, the number of ignitions was closer between the two forcing data sets. Without wind limitation, the ignitions for WATCH were 0.28 times the ignitions for CRUNCEP without wind limitation. After including the wind limitation, the difference between the two forcing data sets decreased, and the

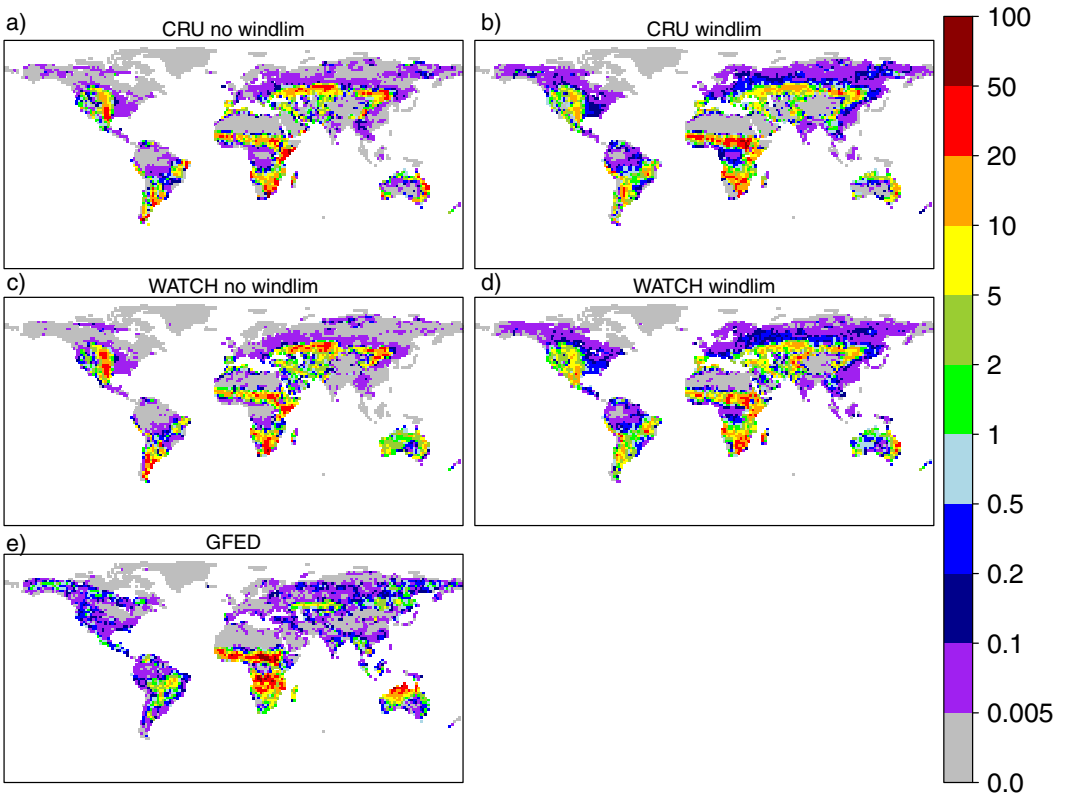

Figure 3. Annual burned fraction averaged for the years 1997–2005 in percent. Model with CRU forcing without (a) and with (b) wind limitation, model forced with WATCH without (c) and with (d) wind limitation, and (e) GFED3.

necessary reduction in ignitions for WATCH were only 0.55 times the ignitions for CRUNCEP. We investigated further how this difference depends on the difference in wind speed of the two forcing data sets, by exchanging the wind speed and limitation parameters of the WATCH forcing with wind speed and parameters of the CRUNCEP forcing. In this case, the ignitions need only be reduced by a factor of 0.74. Therefore, a large part of the difference in the number of ignitions between WATCH and CRUNCEP can be attributed to the influence of wind speed on the rate of spread. The changes in the global distribution of the burned area between simulations with and without wind limitation are qualitatively very similar for both forcing data sets (see Figure 3). The changes include improvements of the global distribution when compared to the GFED3 data set by a reduction of fires in temperate North America, Southern South America, and central Asia. The higher number of ignitions in the wind limited simulations increased the burned fraction in boreal regions and northern Africa, where wind speed is rather low (see Figure 3). An underestimation for very low wind speed remains, which can mainly be attributed to regions in Africa. In southern hemisphere Africa, these regions show a too high tree cover of our prescribed land cover compared to the satellite based observations reported by *Hansen et al.* [2003]. Points with a strong overestimate of tree cover are colored in red in Figures 2e and 2f. This might explain the underestimation. Improvement of the cover fractions of the plant functional types with new satellite data products could therefore improve the modeled burned fraction.

A wind speed limit has been suggested for the Rothermel equations [*Rothermel*, 1972] for which the wind speed modifier, and in consequence also the rate of spread, should be constant for wind speed values higher than a certain limit. The physical explanation behind this limitation is that with higher wind speed the flame angle is less optimal for spread [*Rothermel*, 1972]. Only a maximum, no decrease, for the influence of wind speed has been suggested, although the limit is based on local measurements which show a decrease of the rate of spread for high wind speed. These observations have been reanalyzed and discussed recently and changes in the fuel composition instead of high wind speeds have been suggested as a reason for the decrease [*Andrews et al.*, 2013]. The decrease in the satellite-based observations in burned fraction

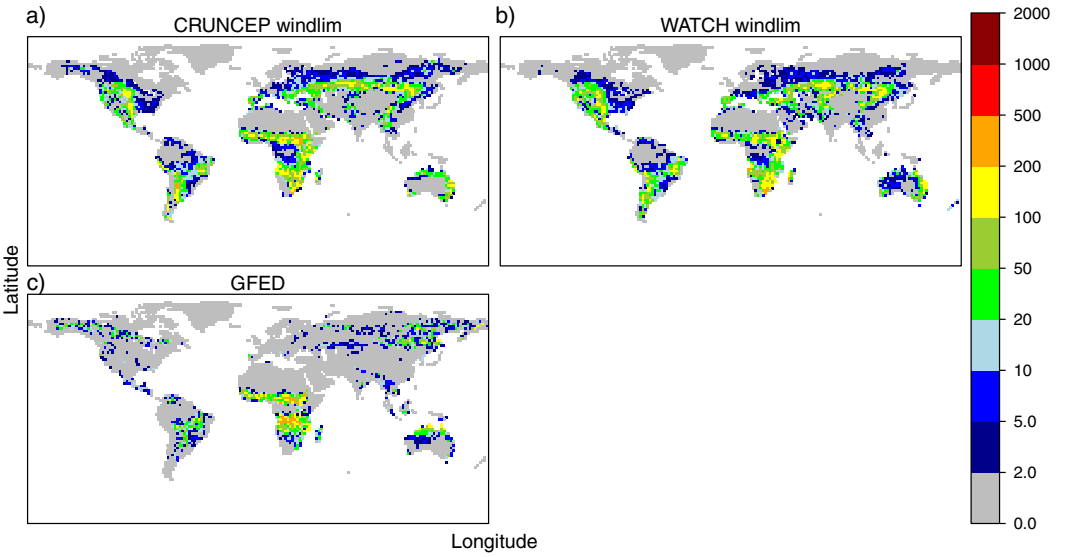

Figure 4. Mean annual carbon emissions (g C m^{-2} $year^{-1}$) averaged for the years 1997–2005. Model with CRU forcing (a), model forced with WATCH (b), and (c) GFED3. For GFED peat, deforestation and cropland fires were excluded.

for high wind speed is strong. A similar relation in the model could only be reached when reducing the rate of spread. The difference in scale might be one explanation why local scale fire modeling might need a different response function to wind speed than global scale models operating on rather coarse grid boxes.

3.2. Model Evaluation

In this section, we compare the model including the wind limitation with observations if not stated otherwise. We first compare the global distribution of annual values for the burned fraction, carbon emissions, and fuel consumption (carbon emissions per burned area). Then, we evaluate the seasonality in terms of the month with the maximum burned fraction and number of months with fires. Based on the benchmarking metrics of *Kelley et al*. [2013], we compare our model versions, with and without wind limitation, to fire models analyzed in their study. The last part of the evaluation shows an analysis of the relation between the difference between model and observations and driving variables.

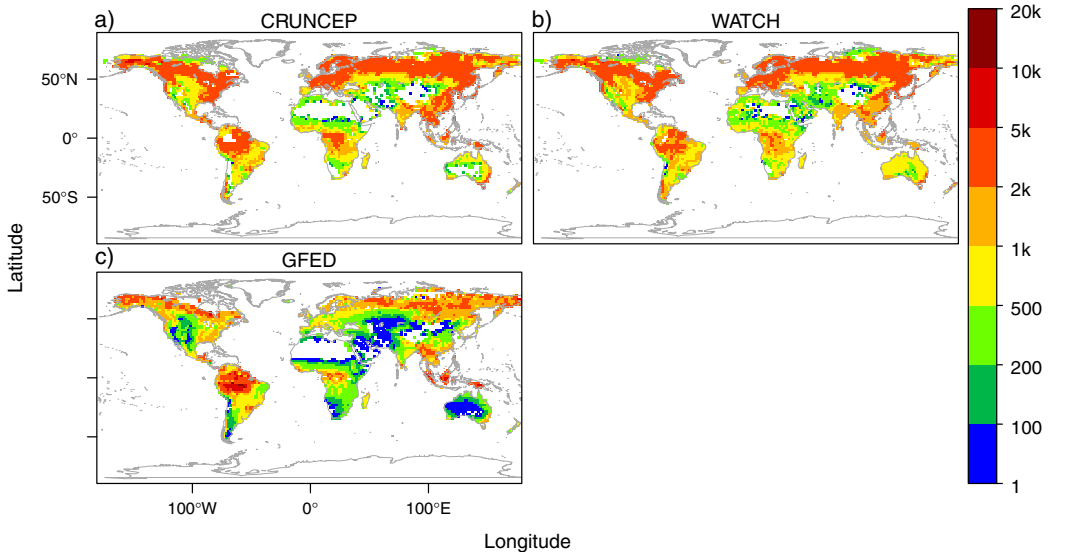

Figure 5. Annual fuel consumption (g C (m^2 burned)$^{-1}$) averaged for the years 1997–2005. Model with CRU forcing (a), model forced with WATCH (b), and (c) GFED3.

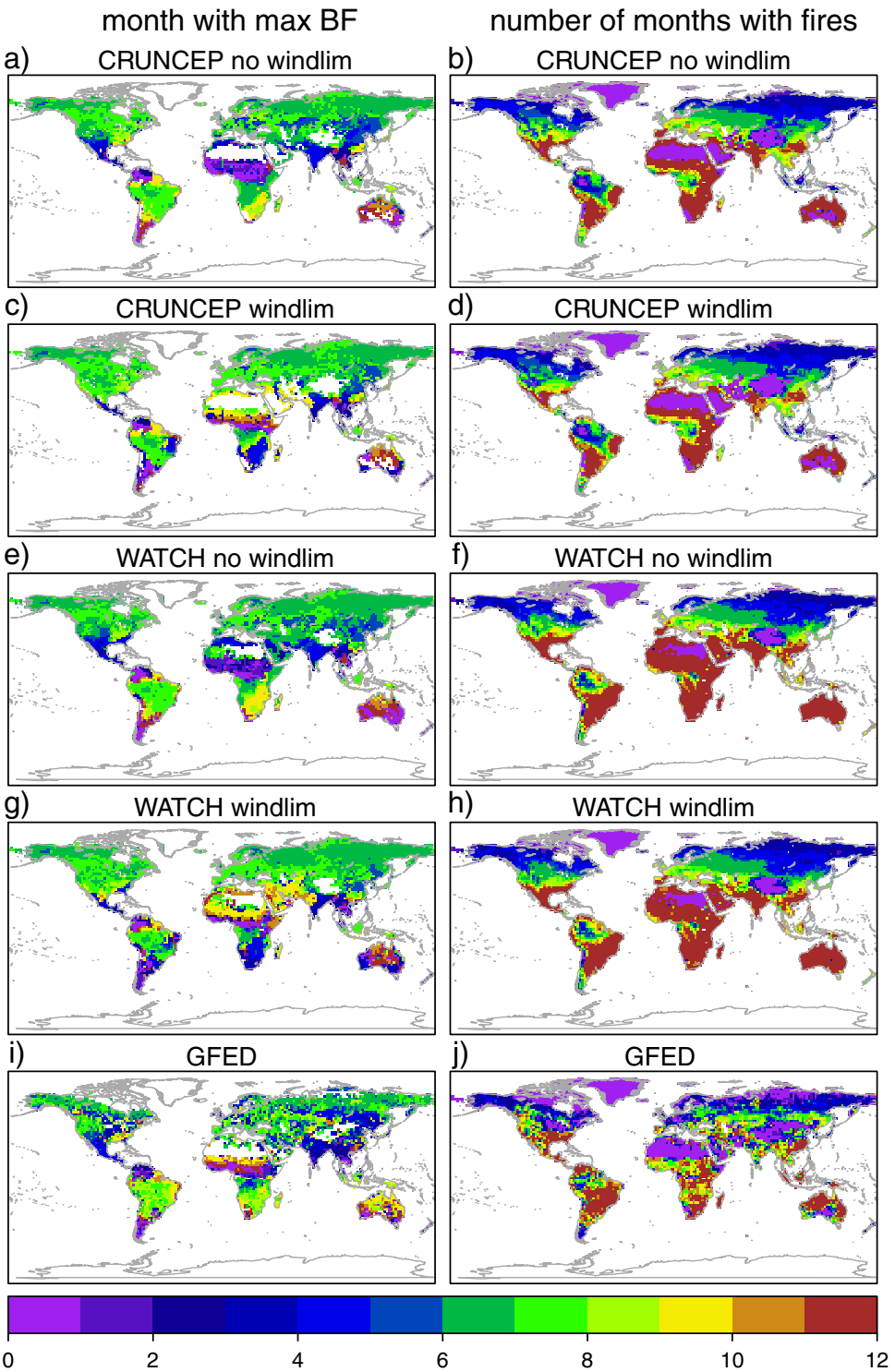

Figure 6. Month with highest burned fraction (left column), number of months with fires (burned area greater than zero) (right column). (a, b) Model forced with CRUNCEP and without wind limitation, (c, d) model forced with CRUNCEP including the wind limitation (e, f) model forced with WATCH and without wind limitation, (g, h) model forced with WATCH including the wind limitation, (i, j) GFED3 satellite data.

The global distribution of burned fraction is similar for the model forced with CRUNCEP and forced with WATCH data (Figures 3b and 3d). Both simulations show the strong dominance of Africa with very high burned fractions. Very low values are simulated for tropical rainforests, deserts, and toward the higher latitude regions. The burned fraction in southern hemisphere Africa, however, is underestimated by the model

Table 3. Benchmarking Scores for the Burned Fraction Compared to *Kelley et al*. [2013], Scores for LPJ and LPX Are Taken From *Kelley et al*. [2013][a]

				JSBACH	JSBACH	JSBACH	JSBACH
						CRUNCEP	WATCH
Metric	Measure	LPJ	LPX	CRUNCEP	WATCH	No windlimit	No windlimit
NME	Annual average	1.58	0.85	0.80	0.87	0.99	1.01
	− mean removed	1.55	0.91	0.80	0.87	0.99	1.01
	− mean + variance removed	1.72	0.99	0.85	0.96	1.01	1.07
NMSE	Annual average	1.18	1.01	0.91	1.00	1.48	1.40
	− mean removed	1.17	1.01	0.90	1.00	1.48	1.40
	− mean + variance removed	1.29	1.60	1.12	1.36	1.73	1.78
NME	Interannual variability	2.86	0.63	1.03	1.04	0.92	0.93
	− variance removed	1.9	0.77	1.56	1.38	1.08	1.38
NMSE	Interannual variability	8.10	0.49	1.33	1.57	0.95	1.21
	− variance removed	3.08	0.56	2.92	2.18	1.26	2.23
NME	Seasonal concentration	-	1.38	1.42	1.56	1.32	1.41
	− mean removed	-	1.38	1.36	1.42	1.22	1.27
	− mean + variance removed	-	1.26	1.07	1.05	1.04	1.04
NMSE	Seasonal concentration	-	2.00	2.25	2.64	1.87	2.11
	− mean removed	-	1.99	1.92	2.02	1.57	1.64
	− mean + variance removed	-	1.77	1.39	1.38	1.30	1.29
MPD	Phase	-	0.10	0.30	0.32	0.27	0.28

[a]The scores are zero for perfect agreement between model and observations. A score of one is achieved when using the observation's mean instead of the model output.

when compared to the GFED3 burned fraction (by a factor of 0.5). For Australia burned fraction is underestimated and over all, the highest burned fractions are simulated in the east, while the data show the highest fractions in the northwest. In temperate North America and central Asia, the model strongly overestimates the burned fraction. Cultural aspects might be an important controlling factor in these regions, which we do not account for in the model. Landscape fragmentation may be an important factor determining the spatial variations, which is neglected in the model. *Pfeiffer et al*. [2013] consider landscape fragmentation in their model for preindustrial fire by approximating the average contiguous area based on the cropland fraction. It remains unclear whether this approach is applicable for the present and in regions with strong anthropogenic influence. Additional factors may be the fuel pattern and slope of the landscape [*Cary et al*., 2006].

The mean annual carbon emissions are higher for the model results (CRUNCEP: 2.44 Pg C year^{-1}, WATCH: 2.54 Pg C year^{-1}) compared to the GFED3 database (1.5 Pg C year^{-1}, excluding peat, deforestation, and cropland fires) (see Figure 4). Our model is still in the range of emission estimates for recent years (*Mieville et al*. [2010]: 2.6 Pg C). In several comparisons, the GFED3 data set was found to be lower than global estimates using other approaches [*Mieville et al*., 2010; *Granier et al*., 2011; *Kaiser et al*., 2012; *Wiedinmyer et al*., 2011]. The higher emissions of our model compared to the GFED3 estimates can have various reasons. The fuel load of our land surface model could be higher compared to the CASA model, used for the GFED3 carbon emission data [*van der Werf et al*., 2010]. The burned fraction is mapped to the PFTs according to their cover fractions, while fire spreads more easily in grasslands. As a consequence, a too high fraction of forests could be burned in our model. In addition, the combustion completeness or mortality of our model could be higher than the ones used in CASA. These parameters are still poorly constrained at the global scale. The burned area was tuned to a global value similar to the observations, but regionally the burned fraction deviates considerably. The model shows higher burned fractions in more productive regions compared to the GFED3 data set. Only cropland fires were excluded from the burned area data set while also deforestation fires and peatland fires were excluded from the carbon emission data, as these processes are not included in the model. Peat fires cover a rather small area and also deforestation fires have rather small burned area, but with very high emissions. Therefore, this inconsistency cannot explain the large difference between our model simulation and the GFED3 data set for the global emissions.

The fuel consumption, which is the carbon emission per burned area, shows similar global gradients for the JSBACH model and GFED3 (Figure 5). The modeled fuel consumption is higher for large regions, which leads to higher carbon emissions. Differences between model and GFED3 estimates are most pronounced in

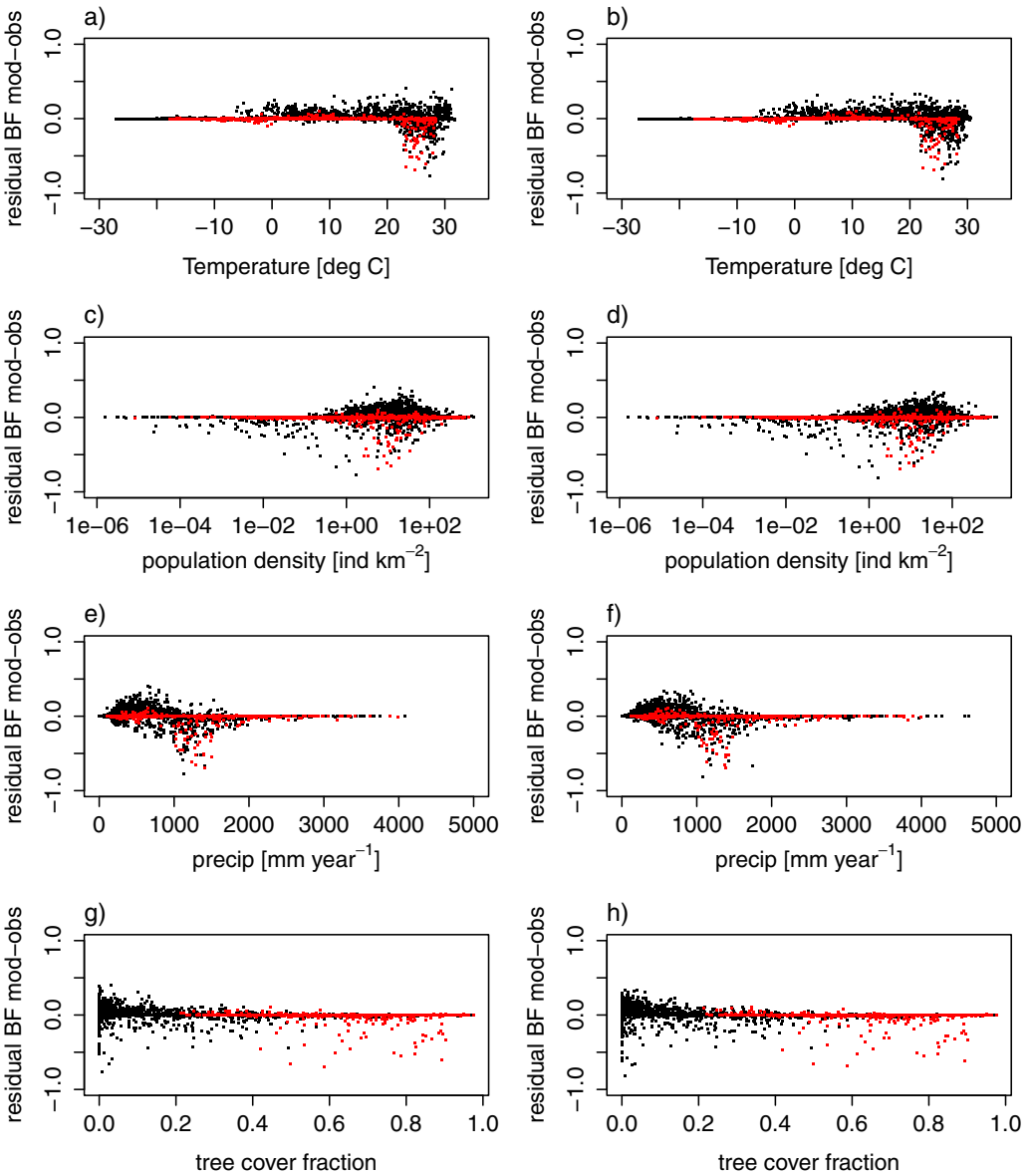

Figure 7. Annual model residual versus four different variables. Left column for CRUNCEP, right column for WATCH forcing. Residuals with a difference between modeled and observed tree cover higher than 0.2 are colored in red.

regions with very low fuel consumption. The model results using the CRUNCEP forcing shows larger areas with near zero fuel consumption than using the WATCH forcing. This indicates that the fuel load might be higher in arid regions when WATCH forcing data are applied in the model. More observations on the fuel consumption could help to validate the GFED3 data set and model approaches.

The global spatial variation in seasonality, i.e., the month with maximum burned area and the number of months with fire, is captured by the model (see Figure 6). When including the wind limitation, the regional gradient across northern hemisphere Africa is reproduced well, while in southern hemisphere Africa the model including the wind limitation shows higher lags. The model runs show larger regions with fires in all 12 months compared to the GFED3 database. For the WATCH forcing arid areas are more productive (see Figure 1), e.g., Australia does not show areas with zero months with fire. For CRUNCEP, the areas with zero months with fire in Australia compare well with the GFED3 data. Without the wind limitation, the average lag is lower, but the seasonality in northern Africa where the burned fraction is highest does not show the gradient from Sahel to tropical forest. Differences between the wind limited and unlimited version are small for the number of months with fire occurrence.

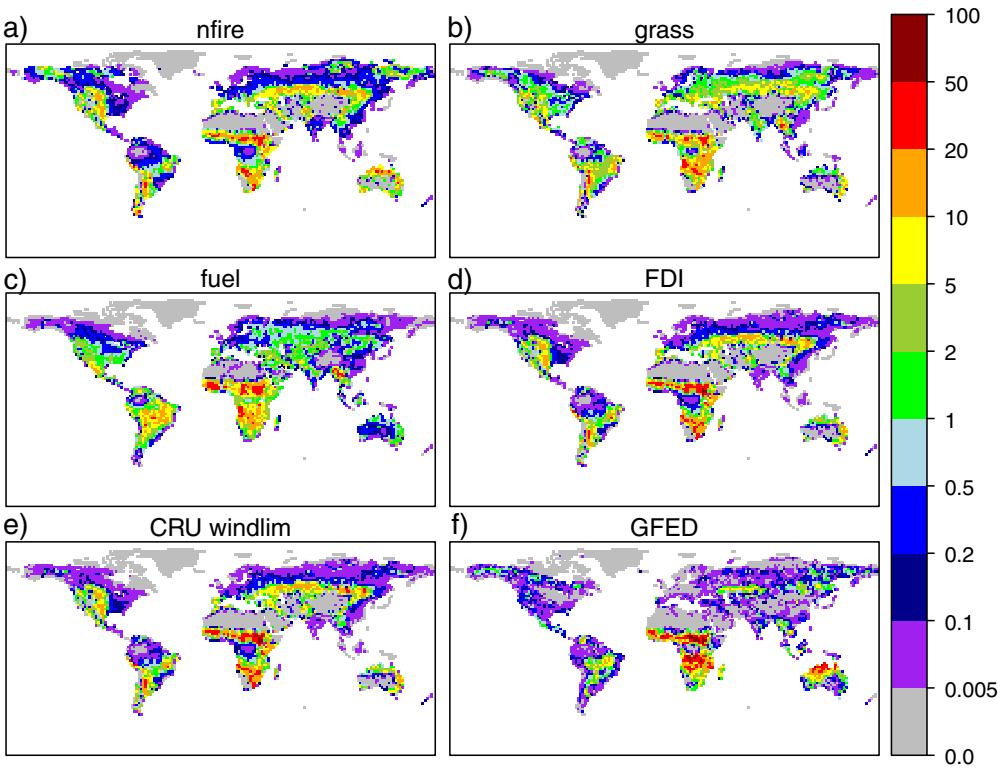

Figure 8. Burned fraction averaged over the years 1997–2005 as result of a globally constant number of fires 0.00002 ha^{-1} (a), only grass cover (b), constant fuel load and composition 78 g biomass m^{-2} for 1,10,100 and 1000 h fuel (c), constant FDI of 0.91 (d). The reference for the simulations in this figure is the run driven with CRUNCEP including the wind limitation (e), which is the same as in Figure 3b. The GFED3 burned fraction for additional comparison is shown in (f).

We further evaluate our model based on the global benchmarking scores suggested by *Kelley et al*. [2013] (see equations ((4–10))) for the burned fraction. The benchmarking of *Kelley et al*. [2013] uses the same burned area data set, but a different spatial resolution ($0.5 \times 0.5^\circ$ compared to 1.875° used in our simulations). Including the wind limitation leads to a strong improvement for the annual averages of burned fraction, while the scores for the interannual and seasonal concentration are slightly diminished (see Table 3). Overall the run forced with CRUNCEP data shows better results across the benchmarking metrics compared to the simulation using WATCH forcing. The scores of LPJ and LPX given in *Kelley et al*. [2013] show a better performance of LPX than of LPJ. The scores of our model, driven either with WATCH or CRUNCEP, also show a better performance compared to LPJ. For the annual average of the burned fraction, the CRUNCEP driven model run has better scores than LPX for all metrics, for WATCH only some of the metrics show a better performance. For the interannual variability, seasonal concentration and phase, LPX shows the best performance for most metrics, only for the seasonal concentration with mean and variance removed our model performs better.

For the seasonal and interannual measures, all grid points enter the metric with equal weights. A revised metric which considers the different magnitudes of burned fraction in each grid cell could be advantageous when computing the final score for temporal variations. In general, the benchmarking scores give a first impression about the model performance. They do, however, not replace a detailed model intercomparison, which is required to understand differences in model behavior.

The residuals between model and data should not show systematic patterns with respect to other variables. If a certain variable can explain variations of the residuals, the response of the model to this variable can be improved in theory. In practice, it usually is difficult to disentangle effects, since the forcing variables are often correlated. Here, we analyze the residuals with respect to four variables: temperature, population density, precipitation, and tree cover (see Figure 7). Residuals of grid cells with a high deviation of modeled to observed tree cover are colored red, to indicate that we already found a reason for the deviation between

model and data. The residuals of the CRUNCEP and the WATCH model run are similar. The residuals show negative values for mean annual temperature higher than 20°C, below 20°C the residuals are positive. We find negative residuals at very low population densities (less than 1 individual per km^2), i.e., for low population density the model underestimates the burned fraction. Population density does not just influence the number of ignitions but also the size of the fires, either directly by fire suppression or indirectly through fragmentation of the landscape. This effect is not included in SPITFIRE. However, the fire duration is limited to a maximum of 4 h and scaled by the fire danger index, while in reality in regions with low population density fires often burns for multiple days [*Dowdy and Mills*, 2012]. *Pfeiffer et al*. [2013] included a fragmentation index based on the fraction of croplands in the grid cell. In addition, net income of a country is related to road density on regional scale [*Wondemu and Weiss*, 2012]. Including either one of these variables might help to improve the representation of fire size on global scale. For precipitation, we find positive residuals for annual values up to 1000 mm, negative residuals occur for mean annual precipitation values between 500 and 2000 mm. Part of the underestimation can be attributed to grid boxes with too high tree cover (points with too high tree cover are colored red). These residuals might be reduced when improving the representation of the cover fractions and should not be interpreted in the residual analysis for variables other than tree cover. Residuals show an overestimation of burned fractions for tree cover values less than 0.2 and underestimation for high tree cover.

Overall the residual analysis shows that the model does not have strong biases with respect to the analyzed driving variables.

3.3. Analysis of Important Drivers for the Spatial Variations in Burned Fraction

We analyzed the importance of ignitions, fire danger index, available fuel, and vegetation composition as drivers of spatial variations in burned fraction by performing a set of simulations where these parameters are set to a globally constant value. The constant values were adjusted to achieve the same global burned area as before. The results of these simulations are compared to the reference simulation (Figure 8e), in which all factors are spatially varying to understand the influence of the respective parameter. The reference simulation is the CRUNCEP driven simulation including the wind limitation. The number of fires was fixed to 0.00002 fires per hectare per day. Fires still need to achieve the necessary fire line intensity of 50 kWm^{-1} to spread. The annual burned fraction (see Figure 8a) increases in the high latitudes and Australia and decreases in Africa. The regional variations in Australia strongly improves considering the comparison of the reference run (Figure 8e) to the observations (Figure 8f). The constant number of fires increases the number of fires in northern Australia about an order of magnitude compared to the modeled number of fires. A very low number of fires can be expected in northern Australia, due to the low population density. The low population density in Australia and low fragmentation of the landscape promote very large fire sizes and long fire durations of up to 100 days [*Dowdy and Mills*, 2012]. These long fire durations and variability in landscape fragmentation are not represented in the model, as global information is not available. No differences to the reference simulation are found when fire intensity is too low for fire to spread. These are cases where fuel or moisture is limiting.

The role of vegetation composition was investigated by performing a model run with only grass land cover. This includes C3 and C4 grassland, crops, and pastures (Figure 8b). The simulation with only grass cover shows smoother gradients. The global gradients are captured in this simulation: The burned fraction decreases toward the very high latitudes, the humid tropical rainforests, and the desert regions. However, the burned fractions are more homogeneous regionally and show fewer areas with extremely high or low burned fractions. This analysis shows that the tree cover is especially important to capture regional variability, in low as well as in high latitudes.

Setting all fuel types to the same globally constant value flattens the gradients and removes the regional hotspots in temperate America and Central Asia and increases fires in regions with low fuel load (Figure 8c). In regions dominated by trees, the burned fraction increases due to a change in fuel composition toward lighter fuels compared to the reference simulation. In South America, the regional patterns using the fixed fuel are closer to the observations than with modeled fuel load. This indicates that an improvement of spatial distribution of fuels might help to improve the burned fraction.

Changes in burned fraction due to a constant FDI are very small and not visible on the logarithmic scale. Effects of the FDI are to reduce the number of fires and the fire duration. These effects seem to be minor. Having the FDI fixed, still fuel moisture can pick up the meteorological limitation for fires. This seems to be the more important controlling factor in the model.

4. Conclusions

We implemented and evaluated the state-of-the-art fire algorithm SPITFIRE within the land surface model JSBACH.

Strong overestimations for the burned area occurred in regions with high wind speeds. The modification of the influence of wind speed on the rate of spread improved the global distribution of burned area.

Overall the model performance with respect to spatial and seasonal variations in burned fraction is good, and comparable to other state-of-the-art fire models.

The amount of carbon emitted per area burned is higher in our model compared to the GFED3 data set [*van der Werf et al*., 2010] which might be caused by multiple factors, e.g., differences in fuel load, combustion completeness, or plant mortality. Further observations of this ratio will be useful to further evaluate the model in this respect. The sensitivity to the meteorological forcing data set was strong but once the global total burned area is adjusted to match the value of the observations the model results using different meteorological forcing are similar, with respect to the spatial and seasonal variation. Wind speed has been found to explain a large part of the difference in our tuning parameter between the two forcing data sets used here. The evaluation and residual analysis showed that improvements of the model in some regions may be possible by improving the response to population density and by improving the tree cover in the model.

By fixing certain variables to a globally constant value, it was possible to assess the importance of these variables to specific spatial features and increased our understanding on the drivers of the spatial variations in burned area within the model. All model runs show similar global gradients with few fires in the boreal, desert, and tropical rainforest regions. The strength of the regional gradients in the burned fraction strongly depends on the vegetation and fuel composition.

The MPI-ESM has now the option to include a mechanistic interactive fire model. This allows us to use the model as a tool to address questions on the interactions of fire within the Earth system, such as influences of climatic changes on fire regimes but also the influences of fire on climate, including emissions of greenhouse gases and aerosols or interactions with the vegetation and surface properties.

Acknowledgments

We acknowlegde the development of the offline JSBACH version by S. Zaehle and G. Schürmann and data processing by S. Zaehle and K. Sickel of the CRUNCEP forcing data set. Further we would like to thank A. Spessa, T. Brücher, and S. Hantson for helpful discussions and A. Spessa for providing the a(N_D) data set. G.L. and S.K. would like to thank the DFG for financial support. We acknowledge the DKRZ for providing excellent computing facilities.

References

Andrews, P. L., M. G. Cruz, and R. C. Rothermel (2013), Examination of the wind speed limit function in the Rothermel surface fire spread model, *Int. J. Wildland Fire*, *22*(7), 959–969, doi:10.1071/WF12122.

Arora, V. K., and G. J. Boer (2005), Fire as an interactive component of dynamic vegetation models, *J. Geophys. Res.*, *110*, G02008, doi:10.1029/2005JG000042.

Bowman, D. M. J. S., et al. (2009), Fire in the Earth system, *Science (New York, N.Y.)*, *324*(5926), 481–484, doi:10.1126/science.1163886.

Brovkin, V., L. Boysen, T. Raddatz, V. Gayler, A. Loew, and M. Claussen (2013), Evaluation of vegetation cover and land-surface albedo in MPI-ESM CMIP5 simulations, *J. Adv. Model. Earth Syst.*, *5*, 48–57, doi:10.1029/2012MS000169.

Cary, G. J., R. E. Keane, R. H. Gardner, S. Lavorel, M. D. Flannigan, I. D. Davies, C. Li, J. M. Lenihan, T. S. Rupp, and F. Mouillot (2006), Comparison of the Sensitivity of Landscape-fire-succession Models to Variation in Terrain, Fuel Pattern, Climate and Weather, *Landscape Ecol.*, *21*(1), 121–137, doi:10.1007/s10980-005-7302-9.

Dowdy, A. J., and G. A. Mills (2012), Characteristics of lightning-attributed wildland fires in south-east Australia, *Int. J. Wildland Fire*, *21*, 521–524, doi:10.1071/WF10145.

Etheridge, D. M., L. P. Steele, R. L. Langenfelds, R. J. Francey, J.-M. Barnola, and V. I. Morgan (1996), Natural and anthropogenic changes in atmospheric CO2 over the last 1000 years from air in Antarctic ice and firn, *J. Geophys. Res.*, *101*, 4115–4128.

Giglio, L., J. T. Randerson, G. R. van der Werf, P. S. Kasibhatla, G. J. Collatz, D. C. Morton, and R. S. DeFries (2010), Assessing variability and long-term trends in burned area by merging multiple satellite fire products, *Biogeosciences*, *7*(3), 1171–1186, doi:10.5194/bg-7–1171-2010.

Giorgetta, M. A., et al. (2013), Climate and carbon cycle changes from 1850 to 2100 in MPI-ESM simulations for the Coupled Model Intercomparison Project phase 5, *J. Adv. Model. Earth Syst.*, *5*, 572–597, doi:10.1002/jame.20038.

Granier, C., et al. (2011), Evolution of anthropogenic and biomass burning emissions of air pollutants at global and regional scales during the 1980 - 2010 period, *Clim. Change*, *109*(1-2), 163–190, doi:10.1007/s10584-011-0154-1.

Hagemann, S., and T. Stacke (2014), Impact of the soil hydrology scheme on simulated soil moisture memory, Springer Berlin Heidelberg, *J. Clim. Dynamics*, 1-20, doi:10.1007/s00382-014-2221-6.

Hansen, M. C., R. S. DeFries, J. R. G. Townshend, M. Carroll, C. Dimiceli, and R. A. Sohlberg (2003), Global percent tree cover at a spatial resolution of 500 meters: First results of the MODIS vegetation continuous fields algorithm, *Earth Interact.*, *7*(10), 1–15, doi:10.1175/1087–3562(2003)007¡0001:GPTCAA¿2.0.CO;2.

Hurtt, G. C., et al. (2011), Harmonization of land-use scenarios for the period 1500–2100: 600 years of global gridded annual land-use transitions, wood harvest, and resulting secondary lands, *Clim. Change*, *109*(1-2), 117–161, doi:10.1007/s10584-011-0153-2.

Kaiser, J. W., et al. (2012), Biomass burning emissions estimated with a global fire assimilation system based on observed fire radiative power, *Biogeosciences*, *9*(1), 527–554, doi:10.5194/bg-9–527-2012.

Keeling, C. D., S. C. Piper, R. B. Bacastow, M. Wahlen, T. P. Whorf, M. Heimann, and H. A. Meijer (2005), Atmospheric CO2 and 13CO2 exchange with the terrestrial biosphere and oceans from 1978 to 2000: Observations and carbon cycle implications, in *A History of Atmospheric CO2 and its Effects on Plants, Animals, and Ecosystems*, edited by J. Ehleringer, T. E. Cerling, and M. D. Dearing, pp. 83–113, Springer, New York.

Kelley, D. I., I. C. Prentice, S. P. Harrison, H. Wang, M. Simard, J. B. Fisher, and K. O. Willis (2013), A comprehensive benchmarking system for evaluating global vegetation models, *Biogeosciences*, *10*(5), 3313–3340, doi:10.5194/bg-10–3313-2013.
Keywood, M., M. Kanakidou, A. Stohl, G. Grassi, C. P. Meyer, K. Torseth, D. Edwards, A. M. Thompson, and U. Lohmann (2013), Fire in the AIR: Biomass burning impacts in a changing climate, *Crit. Rev. Environ. Sci. Technol.*, *43*(1), 40–83.
Klein Goldewijk, K. (2001), Estimating global land use change over the past 300 years, *Global Biogeochem. Cycles*, *15*, 417–443.
Kloster, S., N. M. Mahowald, J. T. Randerson, P. E. Thornton, F. M. Hoffman, S. Levis, P. J. Lawrence, J. J. Feddema, K. W. Oleson, and D. M. Lawrence (2010), Fire dynamics during the 20th century simulated by the Community Land Model, *Biogeosciences*, *7*(6), 1877–1902.
Krawchuk, M. A., and M. A. Moritz (2011), Constraints on global fire activity vary across a resource gradient, *Ecology*, *92*(1), 121–32.
Lehsten, V., K. Tansey, H. Balzter, K. Thonicke, A. Spessa, U. Weber, B. Smith, and A. Arneth (2009), Estimating carbon emissions from African wildfires, *Biogeosciences*, *6*(3), 349–360, doi:10.5194/bg-6–349-2009.
Li, F., X. D. Zeng, and S. Levis (2012), A process-based fire parameterization of intermediate complexity in a Dynamic Global Vegetation Model, *Biogeosciences*, *9*(7), 2761–2780, doi:10.5194/bg-9–2761-2012.
Li, F., B. Bond-Lamberty, and S. Levis (2014), Quantifying the role of fire in the Earth system Part 2: Impact on the net carbon balance of global terrestrial ecosystems for the 20th century, *Biogeosciences*, *11*(5), 1345–1360, doi:10.5194/bg-11–1345-2014.
Marino, E., J.-L. Dupuy, F. Pimont, M. Guijarro, C. Hernando, and R. Linn (2012), Fuel bulk density and fuel moisture content effects on fire rate of spread: A comparison between FIRETEC model predictions and experimental results in shrub fuels, *J. Fire Sci.*, *30*(4), 277–299, doi:10.1177/0734904111434286.
Mieville, A., C. Granier, C. Liousse, B. Guillaume, and F. Mouillot (2010), Emissions of gases and particles from biomass burning during the 20th century using satellite data and an historical reconstruction, *Atmos. Environ.*, *44*, 1469–1477, doi:10.1016/j.atmosenv.2010.01.011.
Pfeiffer, M., A. Spessa, and J. O. Kaplan (2013), A model for global biomass burning in preindustrial time: LPJ-LMfire (v1.0), *Geosci. Model Dev.*, *6*(3), 643–685, doi:10.5194/gmd-6–643-2013.
Pierce, E. (1970), Latitudinal Variation of Lightning Parameters, *J. Appl. Meteorol.*, *9*, 194–195.
Prentice, I. C., D. I. Kelley, P. N. Foster, P. Friedlingstein, S. P. Harrison, and P. J. Bartlein (2011), Modeling fire and the terrestrial carbon balance, *Global Biogeochem. Cycles*, *25*, GB3005, doi:10.1029/2010GB003906.
Raddatz, T. J., C. H. Reick, W. Knorr, J. Kattge, E. Roeckner, R. Schnur, K.-G. Schnitzler, P. Wetzel, and J. Jungclaus (2007), Will the tropical land biosphere dominate the climatecarbon cycle feedback during the twenty-first century?, *Clim. Dyn.*, *29*(6), 565–574, doi:10.1007/s00382-007-0247-8.
Reick, C. H., T. Raddatz, V. Brovkin, and V. Gayler (2013), Representation of natural and anthropogenic land cover change in MPI-ESM, *J. Adv. Model. Earth Syst.*, *5*, 459–482, doi:10.1002/jame.20022.
Rothermel, R. C. (1972), A mathematical model for predicting fire spread in wildland fuels, technical report, USDA For. Serv. Res. Pap. INT-115, USDA (US Department of Agriculture) forest service, Ogden, Utah.
Schneck, R., C. H. Reick, and T. Raddatz (2013), Land contribution to natural CO 2 variability on time scales of centuries, *J. Adv. Model. Earth Syst.*, *5*, 354–365, doi:10.1002/jame.20029.
Shevliakova, E., S. W. Pacala, S. Malyshev, G. C. Hurtt, P. C. D. Milly, J. P. Caspersen, L. T. Sentman, J. P. Fisk, C. Wirth, and C. Crevoisier (2009), Carbon cycling under 300 years of land use change: Importance of the secondary vegetation sink, *Global Biogeochem. Cycles*, *23*, GB2022, doi:10.1029/2007GB003176.
Sitch, S., et al. (2003), Evaluation of ecosystem dynamics, plant geography and terrestrial carbon cycling in the LPJ dynamic global vegetation model, *Global Change Biol.*, *9*(2), 161–185, doi:10.1046/j.1365–2486.2003.00569.x.
Sitch, S., et al. (2013), Trends and drivers of regional sources and sinks of carbon dioxide over the past two decades, *Biogeosci. Discuss.*, *10*(12), 20,113–20,177, doi:10.5194/bgd-10–20113-2013.
Thonicke, K., A. Spessa, I. C. Prentice, S. P. Harrison, L. Dong, and C. Carmona-Moreno (2010), The influence of vegetation, fire spread and fire behaviour on biomass burning and trace gas emissions: Results from a process-based model, *Biogeosciences*, *7*(6), 1991–2011, doi:10.5194/bg-7–1991-2010.
van der Werf, G. R., J. T. Randerson, L. Giglio, G. J. Collatz, M. Mu, P. S. Kasibhatla, D. C. Morton, R. S. DeFries, Y. Jin, and T. T. van Leeuwen (2010), Global fire emissions and the contribution of deforestation, savanna, forest, agricultural, and peat fires (1997–2009), *Atmos. Chem. Phys.*, *10*(23), 11,707–11,735, doi:10.5194/acp-10–11707-2010.
Weedon, G. P., S. Gomes, P. Viterbo, W. J. Shuttleworth, E. Blyth, H. Österle, J. C. Adam, N. Bellouin, O. Boucher, and M. Best (2011), Creation of the WATCH Forcing Data and Its Use to Assess Global and Regional Reference Crop Evaporation over Land during the Twentieth Century, *J. Hydrometeorol.*, *12*(5), 823–848, doi:10.1175/2011JHM1369.1.
Wiedinmyer, C., S. K. Akagi, R. J. Yokelson, L. K. Emmons, J. A. Al-Saadi, J. J. Orlando, and A. J. Soja (2011), The Fire INventory from NCAR (FINN): A high resolution global model to estimate the emissions from open burning, *Geosci. Model Dev.*, *4*(3), 625–641, doi:10.5194/gmd-4–625-2011.
Wondemu, K. A., and J. Weiss (2012), Rural Roads and Development: Evidence from Ethiopia, *Eur. J. Transp. Infrastruc. Res.*, *12*(4), 417–439.
Yue, C., et al. (2014), Modelling fires in the terrestrial carbon balance by incorporating SPITFIRE into the global vegetation model ORCHIDEE Part 1: Simulating historical global burned area and fire regime, *Geosci. Model Dev. Discuss.*, *7*(2), 2377–2427, doi:10.5194/gmdd-7–2377-2014.

Erratum

Figures 2 and 3 were switched in the published manuscript.